A Numerical Investigation of Flame Geometry in Opposed Flow, Thermal Regime Flame Spread over Thin Fuels

Christopher P. Paolini, Ameya Udgaonkar, Subrata Bhattacharjee,
Shuhei Takahashi, and Kazunori Wakai

October 2006

Publication Number: CSRCR2006-01

Computational Science & Engineering Faculty and Students Research Articles

Database Powered by the Computational Science Research Center Computing Group

COMPUTATIONAL SCIENCE & ENGINEERING

SAN DIEGO STATE UNIVERSITY

Computational Science Research Center
College of Sciences
5500 Campanile Drive
San Diego, CA 92182-1245
(619) 594-3430

Manuscript submitted to Prof. R.A. Yetter, Editor, Combustion Science and Technology
Pennsylvania State University
105 Research Building East
University Park, PA 16802-2329

A Numerical Investigation of Flame Geometry in Opposed Flow, Thermal Regime Flame Spread over Thin Fuels

Christopher P. Paolini[1], Ameya Udgaonkar[1], Subrata Bhattacharjee[1], Shuhei Takahashi[2], and Kazunori Wakai[2]

[1] Department of Mechanical Engineering, San Diego State University, San Diego, CA 92182, USA

[2] Department of Mechanical and Systems Engineering, Gifu University, Gifu 501-1193, Japan

E-mail: paolini@engineering.sdsu.edu

Keywords: opposed flow flame spread, flame geometry

Abstract

Although flame spread over solid fuels has been studied for over three decades, the focus has always been the determination of flame spread rate. There have been only a handful of studies directed to the determination of flame shape and structure [3]. In this numerical investigation, our focus is on the flame geometry, especially how the flame shape evolves under varying opposing flow velocity from the quiescent environment of microgravity to blow-off extinction at very high velocity. The ultimate goal of this study is to correlate the flame length, flame stand-off distance, and other flame geometry related variables with known parameters of the problem. Such correlations are important not only from the

stand point of fire safety but also for the development of theory for concurrent-flow flame spread.

Nomenclature

B $\dfrac{\beta_1\beta_2 + 1 - \beta_3}{\beta_4}$

B_g Pre-exponential factor for the gas-phase reaction, $mm^3/kg \cdot s$

c_g Specific heat of gas, kJ/kg·K

c_s Specific heat of solid, kJ/kg·K

Da_s Damkohler number for the pyrolysis reaction, dimensionless; see equation (27)

E Activation energy, $kJ/kmol$

F Flame constant, dimensionless; see equation (6)

g Acceleration due to gravity, 9.8 m/s^2

L_g Gas-phase diffusion length scale, m

L_{gx} Gas-phase diffusion length scale in x-direction, m

L_{gy} Gas-phase diffusion length scale in y-direction, m

L_{sx} Length of the preheated solid phase, m

L_{sy} Thickness of the preheated layer, m

L_v° Latent heat of vaporization, kJ/kg

$\dot{m}_F''$ Fuel mass flux, $kg/m^2 s$

p Pressure, kPa

$\dot{Q}$ Heat flow per unit width, W/m

$\dot{q}''$ Heat flux, W/m^2

R Universal gas constant, 8.315 $kJ/kg \cdot K$

s Stoichiometric air-fuel ratio

$\dot{S}_\phi'''$ Source term for conserved variable ϕ

T_f Characteristic (adiabatic) flame temperature, K

T_v Constant vaporization temperature, K

T_∞ Ambient temperature, K

t_{res} Residence time in gas or solid phase, s

u Gas velocity in the x-direction, m/s

V_g Velocity of the oxidizer, m/s

V_f Absolute spread rate, m/s

V_r Velocity relative to the flame, $V_r = V_g + V_f$

v Gas velocity in the y-direction, m/s

W Width of the fuel in z -direction, m

y_F Mass fraction of fuel

y_{O_2} Mass fraction of oxygen

y_{N_2} Mass fraction of nitrogen

Greek Symbols

α_g Thermal diffusivity of gas evaluated at T_v, m^2/s

α_s Thermal diffusivity of solid, K

β_1 Stoichiometric parameter, $y_{O_2,\infty}/s$

β_2 Dimensionless heat of combustion, $-\Delta h_c^\circ / c_g T_\infty$

β_3 Dimensionless vaporization temperature, T_v / T_∞

β_4 Dimensionless heat of vaporization, $\Delta h_v^\circ / c_g T_\infty$

ε Radiative emittance of the fuel surface

Γ_ϕ Diffusion coefficient for conserved variable ϕ

λ_g Gas-phase conductivity evaluated at T_v, kW/m·K

λ_s Solid-phase conductivity, kW/m·K

ϕ Conserved variable defined in Table 1

ρ_g Gas density evaluated at T_v, kg/m^3

ρ_s Solid density, kg/m^3

τ Fuel half-thickness, m

τ_h Thickness of the heated layer, m

Subscripts

F Fuel

g gas

gsr Gas-to-surface radiation

N Nitrogen

O Oxygen

s Solid

ser Surface-to-environment radiation

w Wall or fuel surface

∞ Ambient conditions

1. Introduction

In this study we extend the earlier results of Bhattacharjee et al. (2004, 1994) in the formulation of opposed flow flame spread to derive simplified functions for geometric attributes of thin fuel flames. As shown in figure 1, an opposed flow flame is one in which the flame propagates in a direction opposite the flow of the oxidizer. In this configuration, a flame propagates by the forward transfer of heat via conduction in the gas phase to the virgin fuel in front of the flame's leading edge. This forward heat transfer raises the fuel's temperature from its ambient temperature T_∞ to its characteristic vaporization temperature T_v. With respect to the flame, the oxidizer is assumed to be a mixture of oxygen and nitrogen and approaches with velocity V_g and the fuel approaches with velocity V_f. The scaling analysis presented in this paper is with respect to two control volumes, one in the gas phase of dimension $L_{gx} \times L_{gy}$ and one in the solid phase of dimension $L_{sx} \times L_{sy}$.

While previous numerical investigations on flame structure involved flames over thermally thick fuels, limited efforts have been made to find closed form solutions for thin fuel flames. In this work we derive three functions for the flame height, denoted L_h, flame length L_f, and pyrolysis length L_p. We seek formulations of L_h, L_f and L_p as a function of V_g, the mean velocity of the opposing oxidizer. However, V_g is a function of L_g, the diffusion length of the gas phase since $V_g = \frac{\alpha_g}{L_g}$. In a scaling analysis we derive a functional linear relationship between L_h, L_f, L_p and L_g. The resulting formulas are

then tested against a comprehensive numerical model to show reasonable agreement between predicted and observed behavior.

2. Mathematical Model

In our numerical approach we separate the gas and solid phases, assume an initial gas to surface radiative heat flux profile $\dot{q}''_{gs}$ and spread rate V_f, then iteratively solve the solid phase energy equation to obtain a spread rate V_f that satisfies our Eigen condition. The solution of the solid phase temperature distribution will provide the necessary wall temperature T_w and mass flow boundary condition $\dot{m}''_F$ to the gas phase. We solve the gas phase energy, momentum, and species mass fraction equations which, in turn, supply the next iterate with an updated gas to surface radiative heat flux profile. Thus, each phase provides a necessary boundary condition for the other. Our desired unknown is the spread rate V_f which appears as an unknown in the solid phase boundary equation. A solution is obtained when V_f has converged to a steady value. The pseudo code shown in Figure 18 outlines the algorithm we use to find the spread rate V_f.

Our mathematical model consists of a set of two-dimensional, steady, elliptic partial differential equations that characterize the conservation of energy, momentum and mass in the gas phase and a two-dimensional, steady ODE to model the conservation of energy and mass in the solid phase. The conservation equations for the total mass of fuel, oxygen, and nitrogen in the gas phase, as well as momentum and energy in the gas phase, can be expressed in canonical form as

$$\frac{\partial}{\partial x}(\rho u\phi)+\frac{\partial}{\partial y}(\rho v\phi)=\frac{\partial}{\partial x}\left(\Gamma_\phi\frac{\partial\phi}{\partial x}\right)+\frac{\partial}{\partial y}\left(\Gamma_\phi\frac{\partial\phi}{\partial y}\right)+\dot{S}_\phi^{'''} \tag{1}$$

by replacing ϕ, Γ_ϕ, and $\dot{S}_\phi^{'''}$ with the terms given in Table 1. Note that we must solve for the mass fraction of nitrogen so we can find the resulting mass fractions of CO_2 and H_2O. The radiation term, calculated using the global balance method, depends on y_{CO_2} and y_{H_2O}. We include the x-direction diffusion term in equation 1 because, at the leading edge of the flame, heat is transferred in the positive x-direction by conduction in the gas phase to the virgin fuel. For thin fuels T_s remains constant across the fuel thickness and is modeled by a one-dimensional energy equation in terms of a variable fuel density ρ_s:

$$-\tau\rho_s c_{p,s}V_f\frac{dT_s}{dx}+\dot{m}_F^{''}\left[\Delta h_V^0+(c_g-c_s)(T_s-T_\infty)\right]=\lambda_g\left.\frac{\partial T}{\partial y}\right|_{y=0^+}+\alpha\dot{q}_{gsr}^{'}-\varepsilon\dot{q}_{ser}^{'} \tag{2}$$

where

$$\dot{m}_F^{''}=A_s\rho_s\tau e^{\frac{-E_s}{RT_s}}=\frac{d}{dx}(\rho_s\tau V_f) \tag{3}$$

This model allows the fuel to burnout downstream when the fuel density reaches a preset burnout value. Note that a fuel with a half-thickness $\tau < L_{sy}$ must be heated uniformly across its thickness and is therefore considered thermally thin. The negative sign in the LHS of the first term of (2) is due to the fact that V_f is the absolute flame spread velocity in a flame-fixed coordinate system and the solid fuel moves in the negative direction with respect to the x-axis. A schematic of the computational domain for solving the flame spread rate problem is given in Figure 2.

3. Numerical Solution

Our overall goal is to correlate the height and length of a flame in an opposed flow configuration, as well as the length of the flame's pyrolysis region with known parameters so we can predict these attributes. Thus, if we are given a fuel, oxidizer, and ambient conditions, we desire the ability to predict how long and how tall a flame will be and additionally the length of the pyrolysis zone. In terms of known parameters, we have fuel conditions such as fuel thickness and fuel type (the results in this paper are based on cellulose fuel), and ambient conditions that characterize the oxidizer such as the mass fractions of nitrogen and oxygen, the velocity of the opposing flow, and pressure. Given these known parameters we want to find equations to estimate L_h, L_f and L_p. These geometric attributes are illustrated in Figure 3. L_h is defined to be the height of the flame with respect to the fuel, L_f is the horizontal length of the flame along the x-axis from the leading edge to the rear of the combustion reaction zone, and L_p is the horizontal length of the region on the fuel surface where pyrolysis occurs. We define the combustion reaction zone to be the surface where the volumetric fuel depletion rate, $\dot{m}_F'''$, is 10% of the maximum value found. See Table 1 for the equation used to find $\dot{m}_F'''$. To solve this problem we perform many experiments in which we numerically calculate L_h, L_f and L_p under different conditions and correlate them to a scale analysis of the known parameters.

4. Computational Results

Several computational simulations were performed for flames in the thermal, microgravity, and chemical kinetics regime. Each simulation was conducted with specific values for oxygen mass fraction and vaporization temperature. The velocity of the oxidizer was varied and the resulting temperature field was plotted. From each temperature plot, the flame height, length, and the pyrolysis length were measured and plotted with respect to a function of diffusion length L_g derived through mathematical scaling operations.

In Figure 4 we see a typical numerical result from simulating a flame burning a thin film of cellulose where the oxidizer is approaching the flame at 30 cm/s. The left image of Figure 4 is a plot of the temperature profile superimposed on a plot showing the reaction rate. In the right image of Figure 4 we see how the surface temperature changes along the x-axis. We measure the pyrolysis length L_p from the point of discontinuity in the surface temperature plot to where fuel mass flux begins. Fuel height L_h and length L_f are measured from the reaction rate contour plot. For each test case, a contour line was drawn on a reaction rate plot where the volumetric fuel depletion rate $\dot{m}_F'''$ is 10% of the maximum value found, as depicted by the small contour ovals in Figure 4.

Heat transfer from radiative effects can be neglected if the velocity of the opposing flow oxidizer is of sufficient magnitude. If these radiative effects can be ignored along with effects resulting from chemical kinetics, the resulting flame spread is said to reside in the thermal regime. Figure 5 shows the fuel mass fraction y_F and

temperature field T as a function of the oxidizer velocity V_g for a flame in the thermal regime where the oxygen mass fraction y_O of the oxidizer is set to 50%. In the chemical kinetics regime, opposing flow velocities of significantly larger magnitude ultimately lead to blow-off and flame extinction. Figure 6 shows the temperature field T as a function of the oxidizer velocity V_g for a flame in the chemical kinetics regime for $y_O = 21\%$. Figure 7 shows the temperature field T as a function of the oxidizer velocity V_g for a flame in the microgravity regime for $y_O = 50\%$.

To correlate the observed numerical data for flames in the thermal regime, we performed the following scale analysis and then use the results from scaling to plot flame height, flame length, and pyrolysis length against different values of oxidizer velocity.

5. Scaling Results

5.1. Derivation of Flame Height L_h

Our first goal will be to derive, through a scaling analysis, an expression for the flame height L_h. To do so, we first observe that all the fuel entering the pyrolysis zone is completely vaporized as illustrated in Figure 8. We can scale the flow of the solid fuel entering the pyrolysis zone given by the expression in the right box with the flow of vaporized fuel in the pyrolysis region given by the expression in the left box. We can then scale the flow of vaporized fuel in the pyrolysis region with the flow of products, $\rho_g V_g L_h y_F$, exiting the trailing region of the flame as illustrated in Figure 9. If we use an infinite rate kinetic approximation we can balance the vaporized fuel being

carried out by convection, given by the expression in the left box of Figure 9, with the flow of vaporizing fuel in the pyrolysis region given by the expression in the right box. The assumption of infinite rate kinetics implies that, at the flame, $y_F = y_O = 0$. From the scaling analysis thus far, we assume that all the fuel entering the pyrolysis zone exits the flame's trailing region**.** Thus if we have a cold flow with no reaction taking place the mass flow rate of fuel being carried out will be $\rho_g V_g L_h y_F$. Since the bulk of species exiting the trailing zone will be fuel and nitrogen, we can make the assumption $y_F \sim (1 - y_{N_2}) \sim y_{O_2,\infty}$. We determine the location of the flame height where the fuel-air reaction is stoichiometric. Using our assumption $y_F \sim y_{O_2,\infty}$, we can represent the mass flow rate of vaporized fuel being carried out by convection, shown in Figure 10, as $\rho_g V_g L_h y_{O_2,\infty}$.

It has been established [1] that an energy balance on the leading edge of a flame is given by

$$\lambda_g \frac{(T_f - T_v)}{L_{gy}} L_{gx} \sim \rho_s c_s \tau V_f (T_v - T_{F,\infty}) \tag{4}$$

$$V_f \sim \frac{\lambda_g}{\rho_s c_s} \frac{T_f - T_v}{T_v - T_{F,\infty}} \frac{L_{gx}}{L_{gy} \tau} \tag{5}$$

We define the dimensionless flame constant *F* as

$$F = \frac{T_f - T_v}{T_v - T_{F,\infty}} \tag{6}$$

and note the gas-phase diffusion length equality

$$L_g \equiv L_{gx} = L_{gy}, \tag{7}$$

preheated solid phase length similarity

$$L_{sx} \sim L_g = \frac{\alpha_g}{V_r} \tag{8}$$

and the expression for the gas phase diffusivity evaluated at the vaporization temperature

$$\alpha_g = \frac{\lambda_g}{\rho_g c_g}. \tag{9}$$

From (5) we now have an expression for the velocity of a spreading flame over a thin fuel

$$V_{f,thin} \sim= L_{sx} \frac{\rho_g c_g V_r F}{\rho_s c_s \tau} \tag{10}$$

From (8), we have

$$L_{sx} V_r \sim L_g V_r \sim \alpha_g \tag{11}$$

and can rewrite (10) as

$$V_{f,thin} \sim \alpha_g \frac{\rho_g c_g}{\rho_s c_s \tau} F. \tag{12}$$

Further, from (9) we can write

$$\lambda_g = \alpha_g \rho_g c_g \Rightarrow V_{f,thin} \sim \frac{\lambda_g}{\rho_s c_s \tau} F. \tag{13}$$

From the fuel mass balance derivation illustrated in figures 7, 8, and 9, we have

$$\rho_g V_g L_h y_{O_2,\infty} \sim \rho_s \tau V_f \tag{14}$$

and thus we can scale flame height as

$$L_h \sim \frac{\rho_s \tau}{\rho_g V_g} \frac{\lambda_g}{\rho_s c_s \tau} F \frac{1}{y_{O_2,\infty}} \sim \frac{c_g}{c_g} \frac{\lambda_g}{\rho_g V_g c_s} F \frac{1}{y_{O_2,\infty}} \sim \frac{c_g \alpha_g}{V_g c_s} F \frac{1}{y_{O_2,\infty}} \tag{15}$$

However, noting

$$\frac{\alpha_g}{V_g} = L_g, \tag{16}$$

we can express (15) as

$$L_h \sim \left(\frac{c_g}{c_s}\right)\left(\frac{F}{y_{O_2,\infty}}\right) L_g \sim \left(\frac{F}{y_{O_2,\infty}}\right) L_g \tag{17}$$

where we take $\left(\frac{c_g}{c_s}\right)$ as a constant. Finally, we can scale L_h in terms of known temperature, diffusivity, and velocity parameters,

$$L_h \sim \frac{F L_g}{y_{O_2,\infty}} = \frac{\left(T_f - T_v\right)\alpha_g}{y_{O_2,\infty}\left(T_v - T_\infty\right) V_g} \tag{18}$$

5.2 Derivation of Flame Length L_f

In addition to flame height, we wish to derive an expression for flame length L_f. As illustrated in Figure 11, using a simple scale analysis from a balance of oxygen flow through diffusion with the product of the stoichiometric air-fuel ratio *s* and fuel flow rate $\dot{m}_F$ we can write

$$L_f \rho_g D \frac{(y_{O_2,\infty} - 0)}{L_h} \sim s\, \dot{m}_F \sim s\, \tau \rho_s V_f \sim s\, \tau \rho_s \frac{\lambda_g}{\rho_s c_s \tau} F \tag{19}$$

where D is the coefficient of oxygen diffusivity given by

$$D = \frac{\lambda_g}{\rho_g c_g}. \tag{20}$$

Simplifying (19), we obtain a relation for the ratio $\frac{L_f}{L_h}$,

$$\frac{L_f}{L_h} \sim s \frac{\lambda_g}{c_s} F \frac{1}{\rho_g} \frac{1}{y_{O_2,\infty}} \frac{\rho_g c_g}{\lambda_g} \sim s \left(\frac{c_g}{c_s} \right) \left(\frac{1}{y_{O_2,\infty}} \right) F \tag{21}$$

Substituting (18) in (21) for L_h, we obtain a scaled expression for L_f

$$L_f \sim s \left(\frac{c_g}{c_s} \right)^2 \left(\frac{F}{y_{O_2,\infty}} \right)^2 L_g \sim \left(\frac{F}{y_{O_2,\infty}} \right)^2 L_g \tag{22}$$

where the stoichiometric air-fuel ratio s is constant for a given fuel. We can then express L_f in terms of known parameters,

$$L_f \sim \left[\frac{T_f - T_v}{y_{O_2,\infty} \left(T_v - T_\infty \right)} \right]^2 \frac{\alpha_g}{V_g} \tag{23}$$

5.3 Derivation of Pyrolysis Length L_p

To find an expression for the pyrolysis length L_p, we balance the heat transfer through gas to fuel heat conduction in the gas phase with the latent heat that is absorbed as the

fuel is vaporized. The latent heat of vaporization, denoted L_v^0, is the heat absorbed when the fuel changes phase from liquid to gas. This heat transfer scenario is illustrated in Figure 12. We assume the virgin fuel that enters the pyrolysis region is completely vaporized and swept away by the opposing flow. We can express this energy balance as

$$\lambda_g \frac{(T_f - T_v)}{L_h} L_p \sim L_v^0 \dot{m}_F \sim L_v^0 \rho_s \tau V_f \tag{24}$$

Substituting (13) for V_f into (24) we obtain

$$L_p \sim L_h \frac{1}{\lambda_g} \frac{1}{T_f - T_v} L_v^0 \rho_s \tau \frac{\lambda_g}{\rho_s c_s \tau} F \sim \frac{L_v^0}{c_s (T_f - T_v)} F L_h. \tag{25}$$

We obtain a final expression for pyrolysis length in terms of known parameters by substituting (6) for F in (25) yielding

$$L_p \sim \frac{L_v^0}{c_s (T_f - T_v)} \left(\frac{T_f - T_v}{T_v - T_\infty} \right) L_h. \tag{26}$$

The dimensionless Damkohler number for the pyrolysis reaction is defined as

$$Da_s = \frac{c_s \left(T_v - T_\infty \right)}{L_v^0} \tag{27}$$

and represents the ratio of the characteristic residence time (in seconds) of the gas in the preheat zone to the combustion chemical time. Rewriting (26) in terms of Da_s and substituting (18) for L_h, we obtain a final scaling expression for pyrolysis length L_p,

$$L_p \sim \frac{1}{Da_s} L_h \sim \frac{F}{Da_s y_{O_2,\infty}} \left(\frac{c_g}{c_s} \right) L_g \tag{28}$$

In terms of known parameters we express L_p as,

$$L_p \sim \frac{L_v^0 \left(T_f - T_v \right) \alpha_g}{c_s (T_v - T_\infty)^2 y_{O_2,\infty} V_g} \tag{29}$$

5.4 Numerical Results

In Figure 13, Figure 14, and Figure 15 we have plotted the relations given by equations (18), (23) and (29) for L_h, L_f and L_p, respectively. Superimposed on these three graphs, we have plotted the flame height, flame length, and pyrolysis length from the results of performing several numerical simulations. Prior to running a simulation, we defined a baseline configuration, then alter the baseline by changing a particular parameter such as the fuel thickness τ, oxygen mass fraction y_{O_2}, vaporization temperature T_V, or pressure p, and then run a simulation. Our chosen baseline configuration is $\tau = 82.55 \mu m$, $y_{O_2} = 50\%$, $T_v = 789 K$, $p = 1.5\ atm$, and fuel = cellulose. Following each simulation we measured L_h, L_f, L_p and plotted our results. To show our scaled relations are independent of the amount of oxygen in the oxidizer and the characteristic vaporization temperature of the fuel, we varied y_O, T_V, τ, and p, respectively, for each simulation. Each data point corresponds to a different value of V_g and a unique symbol is used to represent the results for each selected value of y_O, T_V, τ, and p.

In Figure 13 we see a strong correlation between the numerically measured flame height and the expression we obtained through scaling given by (18). The R-squared value, a number between 0 and 1, indicates how closely the estimated values for the L_h trend line correspond to our actual data. The trend line is most reliable when its R-squared value is at or near 1. As shown in Figure 13, $R^2 \approx 0.9996$. In Figure 14 we again see the appearance of a strong correlation between flame length and its respective expression we obtained through scaling given by (23). However, in Figure 15 we see the presence of a very poor correlation between L_p and the expression we derived through scaling given by (29). After investigating what may have possibly gone wrong in our derivation (29) for L_p, we concluded that L_h is not a good representation of the flame height at the end of the pyrolysis region because the true height of the flame above the pyrolysis region will be less than the height of the flame at the trailing edge. This difference is illustrated in Figure 17. We therefore decided to scale the pyrolysis length based on the height of the flame at the end of the pyrolysis region and termed this height $L_{h,p}$. To derive an expression for $L_{h,p}$, we assume that as the vaporized fuel is carried away by the opposing flow, the volume enclosed by the flame above the pyrolysis region will be saturated with vaporized fuel since the vaporizing fuel will displace oxygen and nitrogen in the volume above the pyrolysis region. This assumption implies the mass fraction of fuel will be near 1 in the volume enclosed by the flame directly above the pyrolysis zone, as depicted by the grey region in Figure 17.

Deriving an updated expression for L_p using the same scale analysis as before, but replacing L_h with $L_{h,p}$ based on the assumption that $y_F = 1$ instead of $y_F \sim y_{O_2,\infty}$, we can write

$$\rho_g V_g L_{h,p} y_F \sim \rho_g L_{h,p} V_w \sim \rho_s \tau V_f \text{ where } y_F = 1 \Rightarrow L_{h,p} \sim \left(\frac{c_g}{c_s}\right) F L_g \tag{30}$$

This modification will yield a new expression for L_p in terms of a diffusion length $L_g = \frac{\alpha_g}{V_g}$ that is no longer a function of oxygen mass fraction. In terms of known parameters, this is expressed as

$$L_p \sim \frac{L_v^0 \left(T_f - T_v\right) \alpha_g}{c_s (T_v - T_\infty)^2 V_g} \tag{31}$$

In Figure 16 we see the numerical results of L_p correlated with the expression based on $L_{h,p}$ given by (31). Comparing Figure 15 and Figure 16, we see a much better correlation between pyrolysis length and our derivation based on $L_{h,p}$.

6. Conclusions

In conclusion, our results obtained from the numerical simulation of flames in the thermal regime closely coincide with those predicted by the relations we derived through a scaling analysis given by equations (18), (23) and (29) for L_h, L_f, and L_p,

respectively. We developed three significant formulas that reproduce our results for many different conditions. The individual data points obtained by varying V_g fall reasonably close to the $L_h - L_g$, $L_f - L_g$, and $L_p - L_g$ trend lines. We have thus provided some initial supporting evidence that fundamental geometric attributes of flames in an opposed flow configuration over thin fuels in the thermal regime can be reasonably predicted using a simplified scale analysis. The ability to reasonably approximate geometric characteristics of spreading flames can be valuable in fire safety applications.

The flame height to pyrolysis length and flame height to length ratios are interesting to mention. From (18) and (29), we can express the height to pyrolysis length ratio as

$$\frac{L_h}{L_p} \approx 0.4 \frac{Da_s}{y_{O_2,\infty}}. \tag{32}$$

Also, from (18) and (23) we can express the flame height to length ratio as

$$\frac{L_h}{L_f} \approx 6.67 \frac{F}{y_{O_2,\infty}}. \tag{33}$$

References

[1] Bhattacharjee, S., King, M., and Paolini C., Structure of downward spreading flames: A comparison of numerical simulation, experimental results and a simplified parabolic theory, *Combustion Theory and Modeling*, **8**, 2004, 23-39.

[2] Bhattacharjee, S., Bhaskaran, K. K., Altenkirch, R. A., Effects of Pyrolysis kinetics on opposed-flow flame spread modeling, *Combustion Science and Technology*, **100**, 1994, 163-182.

[3] Kumar, A., Tolejko, K., and T'ien, J. S., A computational study on flame radiation-surface interaction in flame spread over thin solid-fuel, *The 6th ASME-JSME Thermal Engineering Joint Conference*, **TED-AJ03-327**, 2003.

[4] Paolini, C., Udgaonkar, A., Bhattacharjee, S., Takahashi, S., and Wakai, K., A Numerical Investigation of Flame Geometry in Opposed Flow Flame Spread over Thin Fuels, *5th Asia-Pacific Conference on Combustion*, Adelaide, Australia, July 2005.

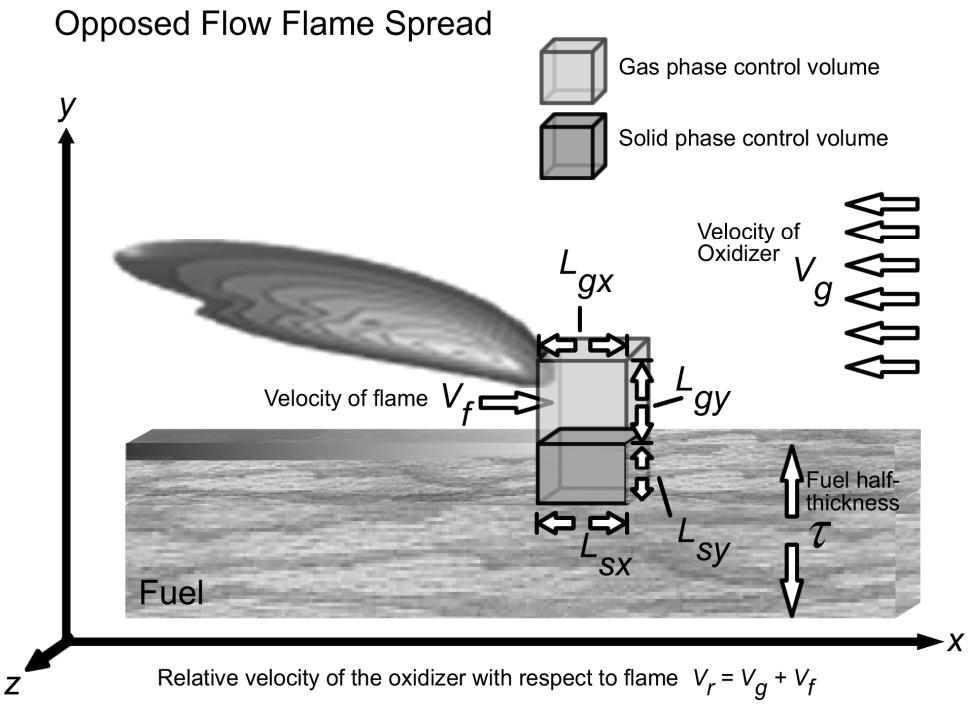

Figure 1. Flame in an opposed flow configuration.

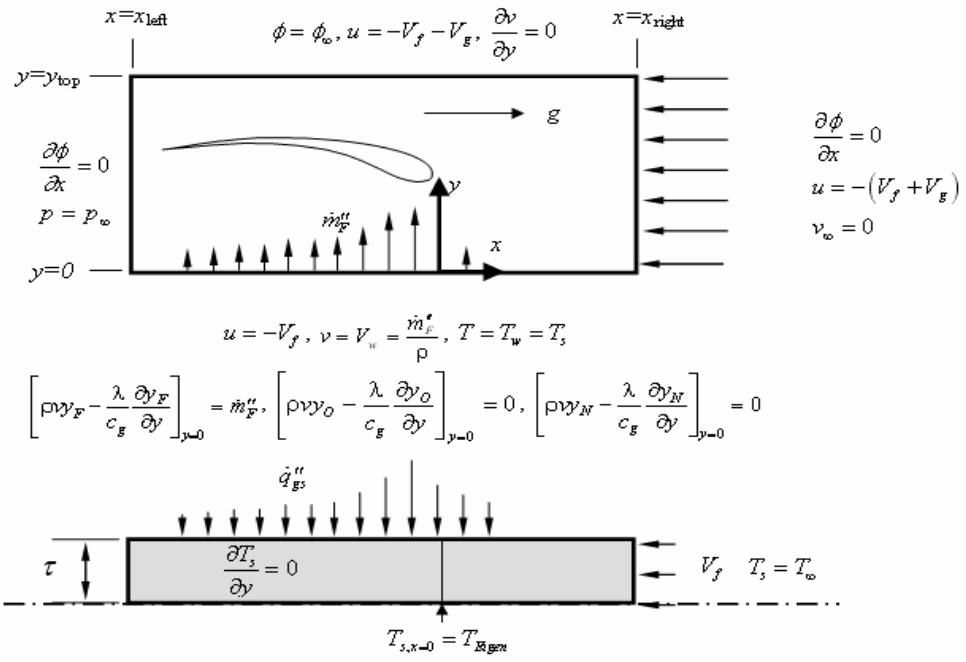

Figure 2. Diagram of computational domain, showing the separation of the gas and solid phases and boundary conditions.

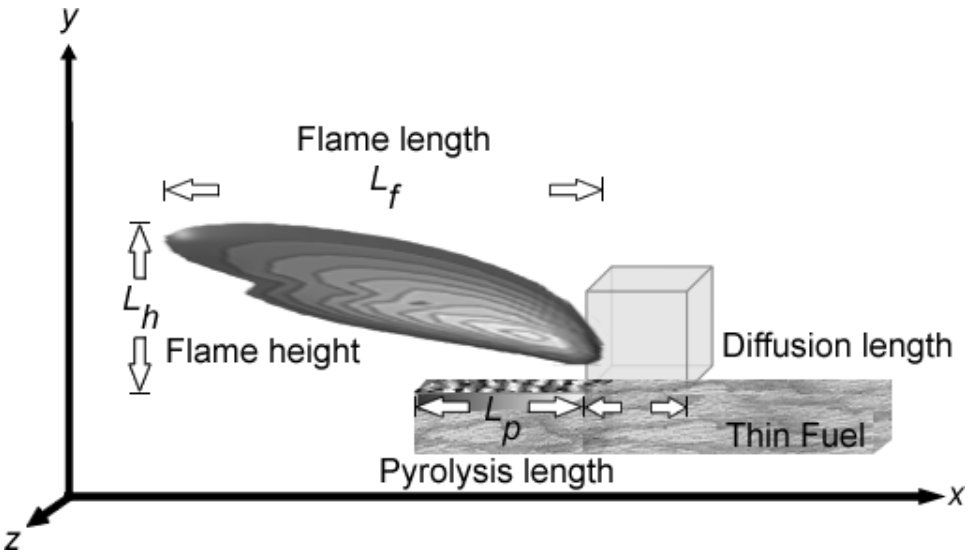

Figure 3. Geometric attributes of a thermal regime flame

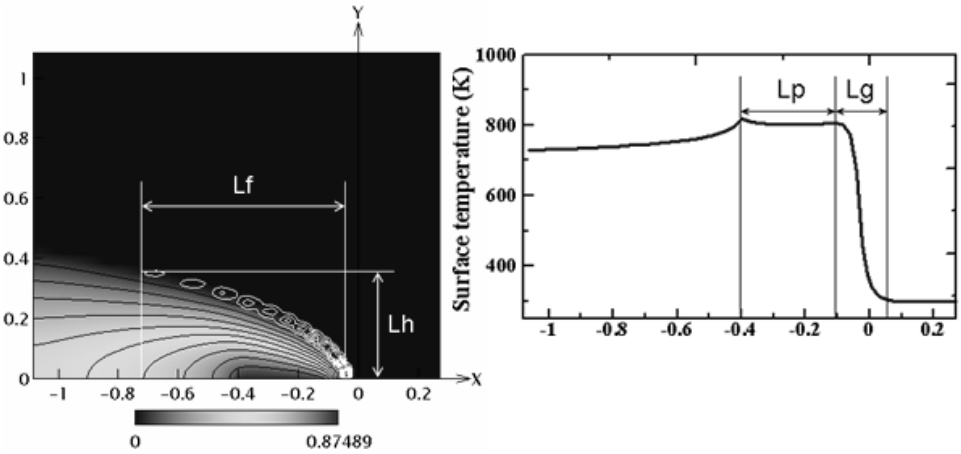

Figure 4. A typical numerical result from simulating a flame burning on a thin film of cellulose.

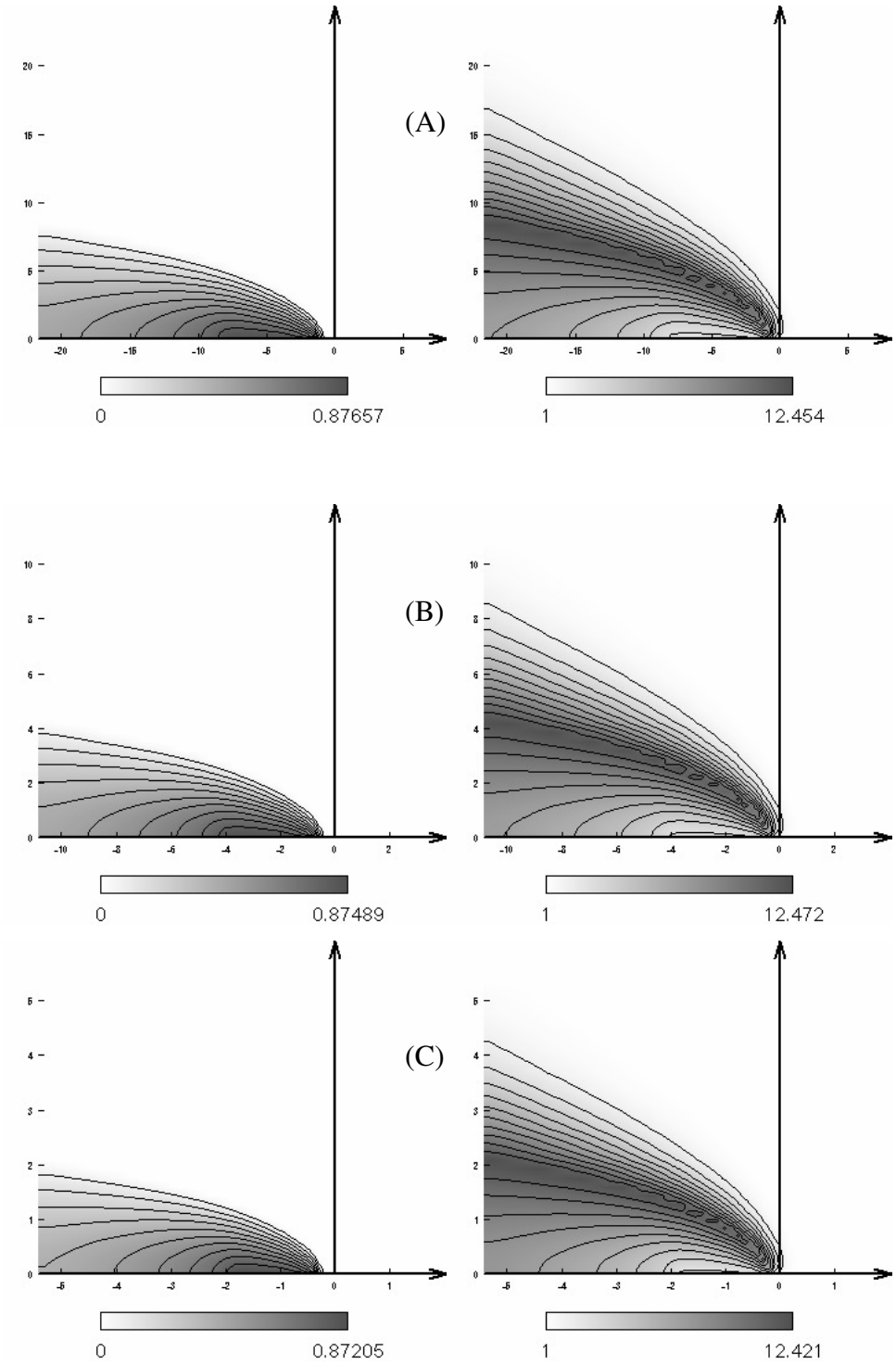

Figure 5. Numerical results for flame spread in the thermal regime. Fuel mass fraction (left) and temperature (right) for $V_g = 15\frac{cm}{s}$ (a), $V_g = 30\frac{cm}{s}$ (b), and $V_g = 60\frac{cm}{s}$ (c). Units on x-y axis in mm.

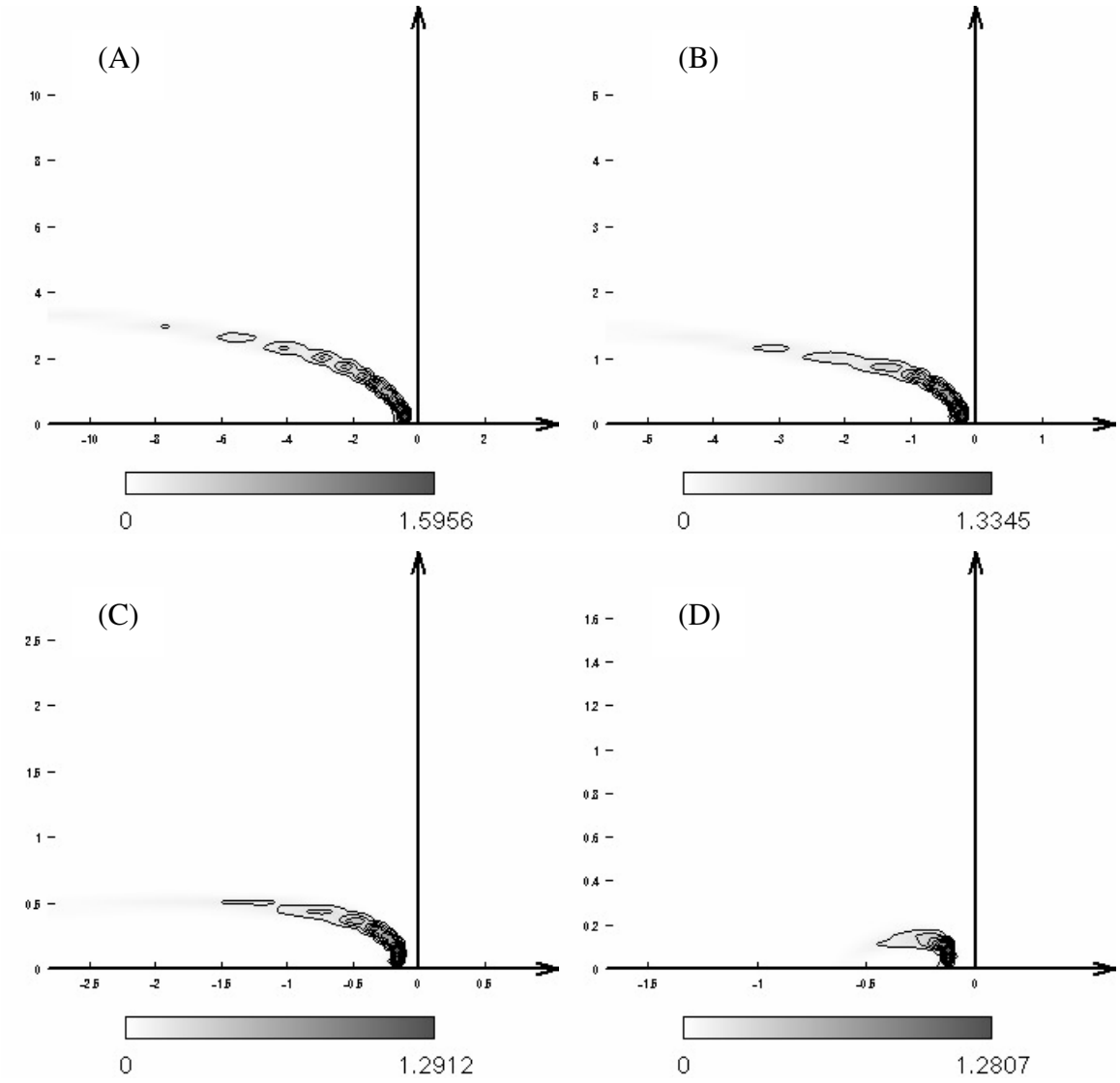

Figure 6. Numerical results for flame spread in the chemical kinetics regime. Temperature field for $V_g = 30\frac{cm}{s}$ (a), $V_g = 60\frac{cm}{s}$ (b), $V_g = 120\frac{cm}{s}$ (c), and $V_g = 200\frac{cm}{s}$ (d). Units on x-y axis in mm.

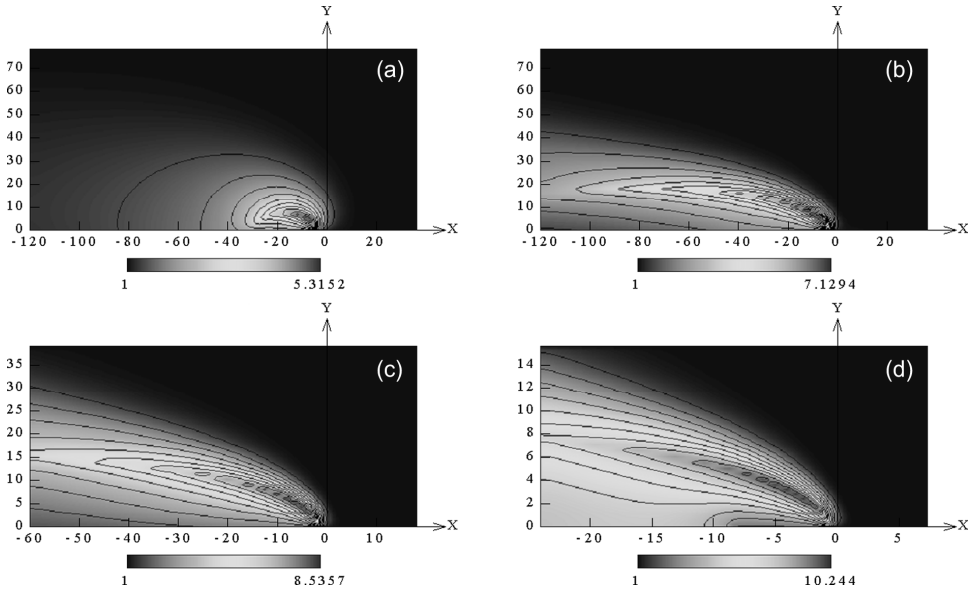

Figure 7. Numerical results for flame spread in the microgravity regime. Temperature field for $V_g = 0\frac{cm}{s}$ (a), $V_g = 3\frac{cm}{s}$ (b), $V_g = 6\frac{cm}{s}$ (c), and $V_g = 15\frac{cm}{s}$ (d). Units on x-y axis in mm.

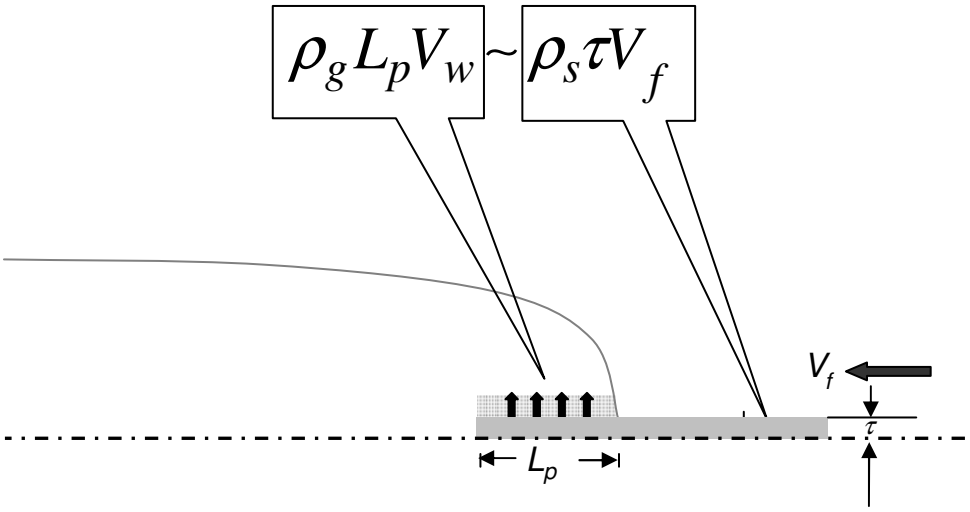

Figure 8. Scaling the flow of solid fuel entering the pyrolysis zone with the flow of vaporized fuel in the pyrolysis region.

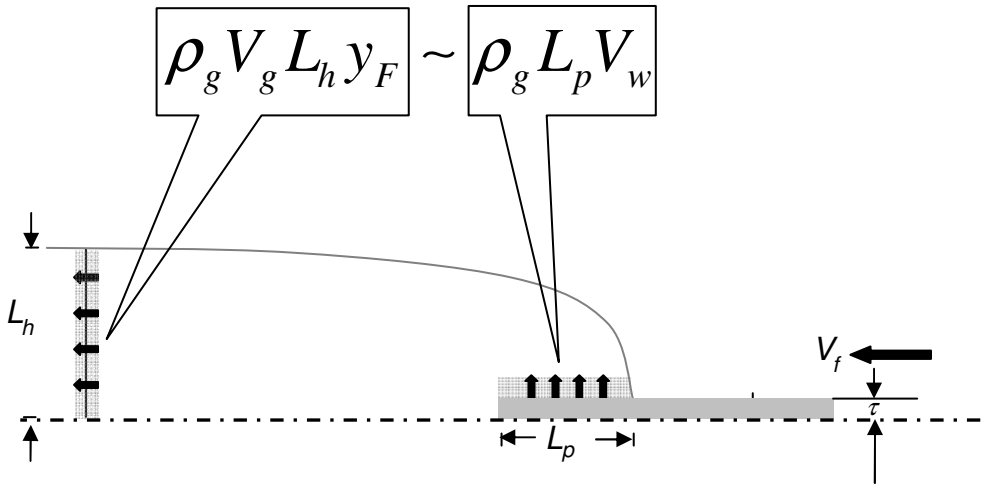

Figure 9. Scaling the flow of vaporized fuel in the pyrolysis region with the flow of products exiting the trailing region.

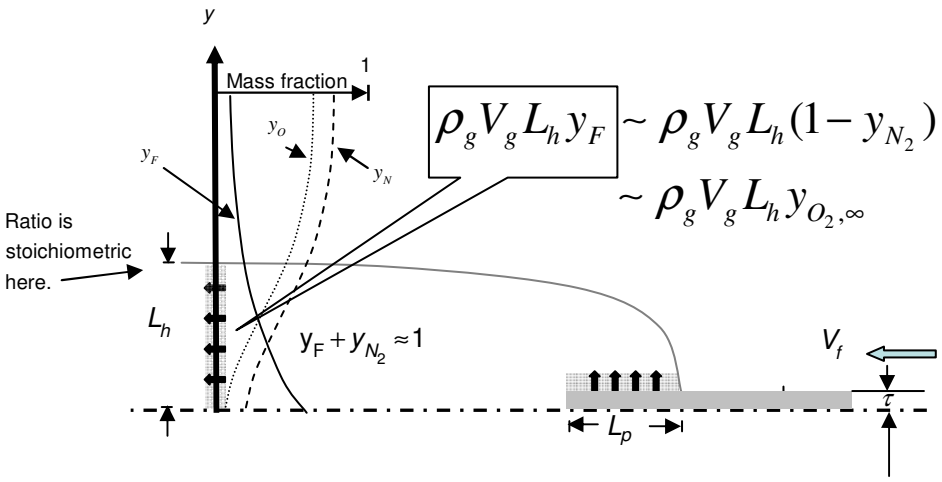

Figure 10. Scaling the flow of vaporized fuel in the trailing region being carried out by convection.

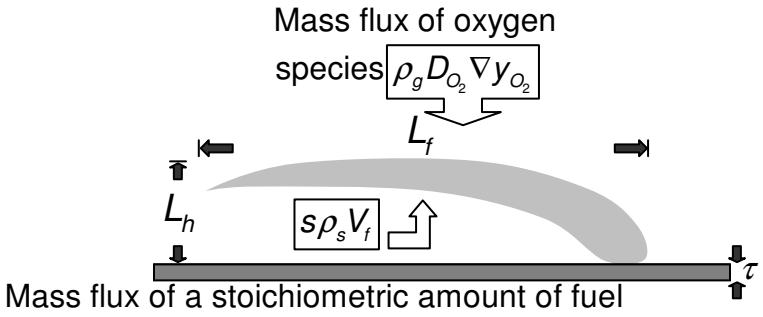

Figure 11. Balancing oxygen flow through diffusion with the product of the stoichiometric air-fuel ratio and the fuel flow rate.

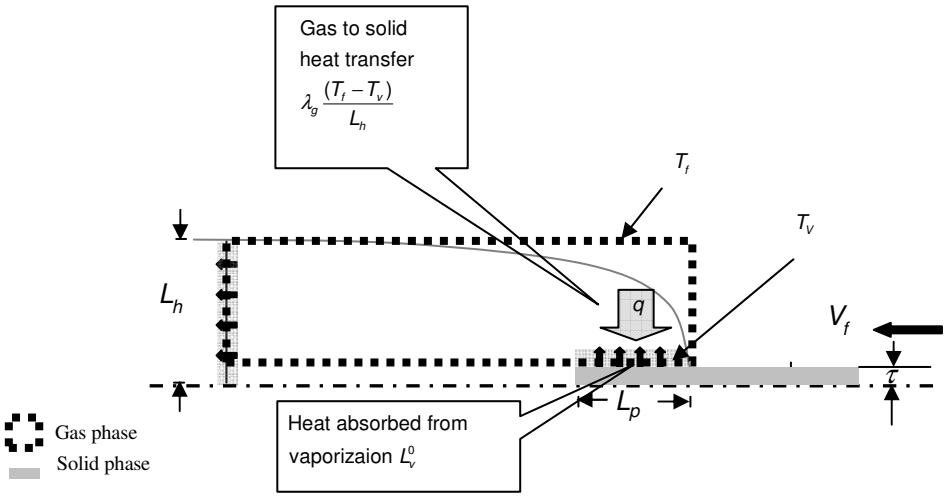

Figure 12. Balancing the gas-to-solid heat transfer with heat absorbed from vaporization.

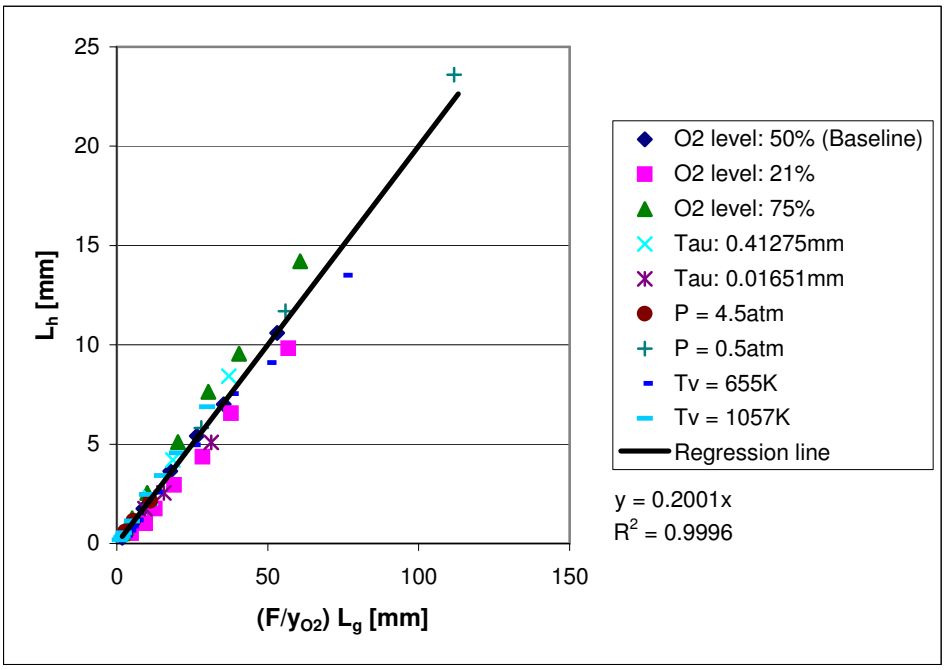

Figure 13. Numerical Results for L_h

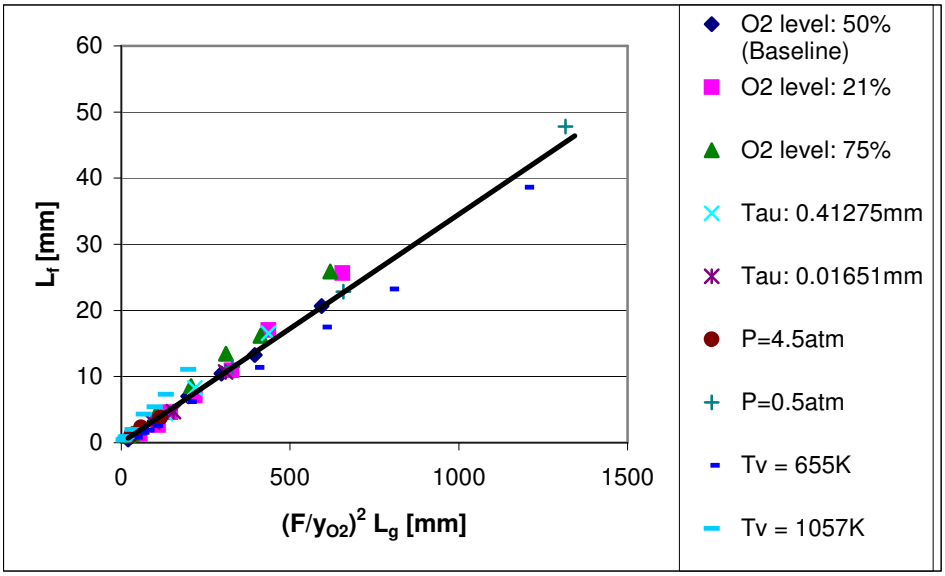

Figure 14. Numerical Results for L_f

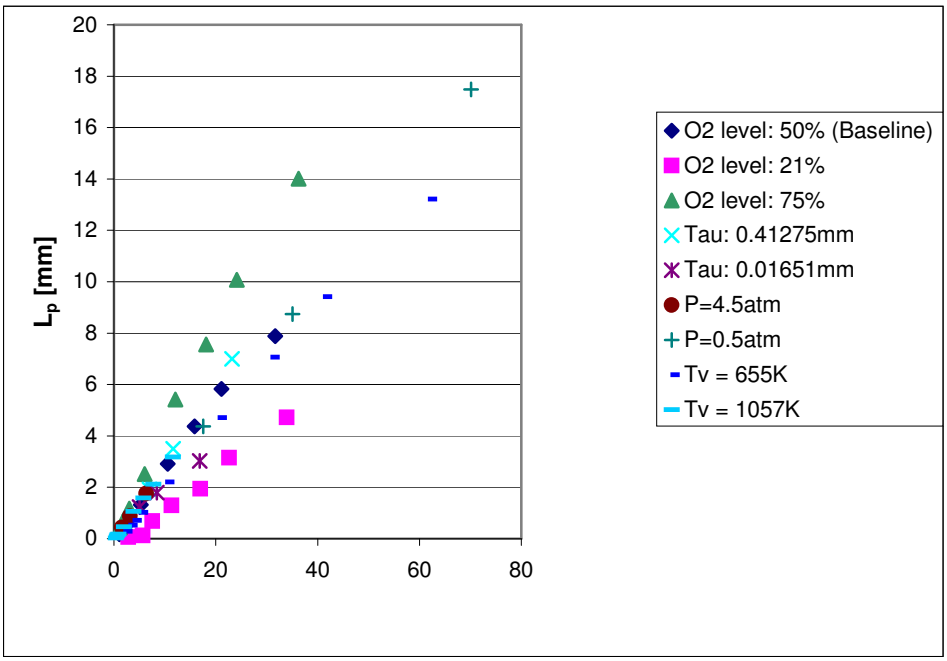

Figure 15. Numerical Results for L_p

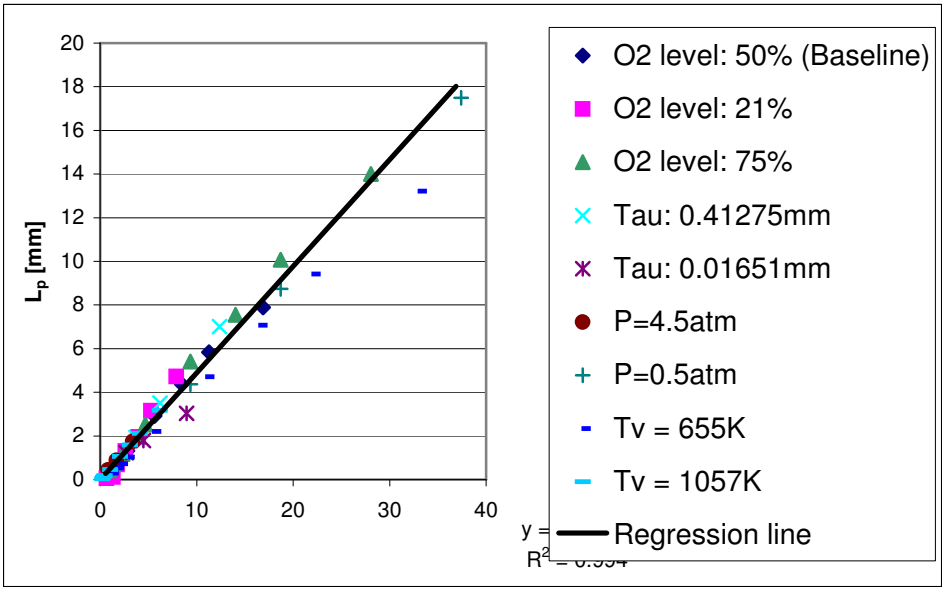

Figure 16. Numerical Results for L_p based on $L_{h,p}$

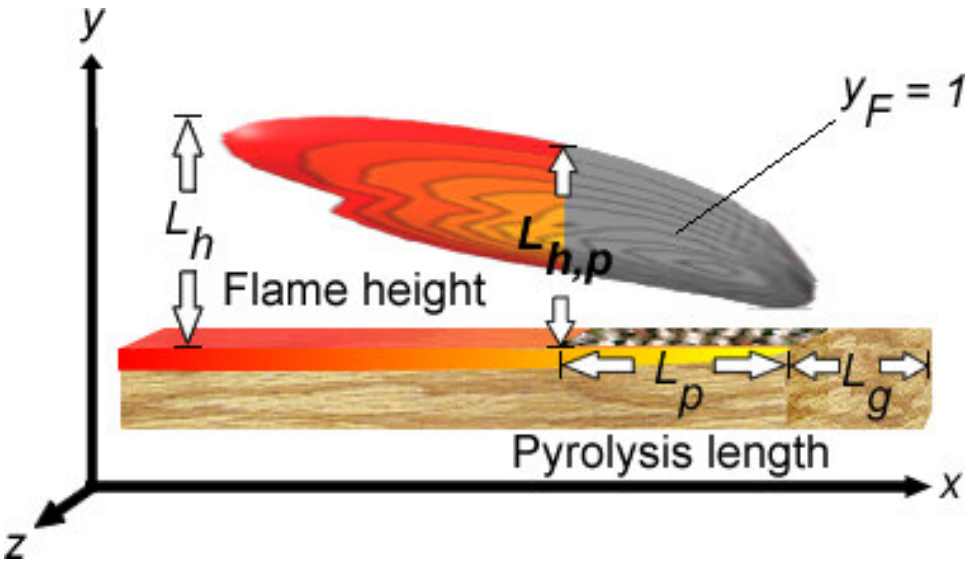

Figure 17. $L_h > L_{h,p}$

$\dot{q}''_{gsr}(x) \Leftarrow \dot{q}''^{,0}_{gsr}(x)$ {Assume an initial gas-to-surface radiative heat flux profile}

loop

{Solve the solid phase energy ODE to obtain a V_f that satisfies the Eigen condition}

$V_f = V_f^0$ {Assume initial value for the flame velocity}

repeat

Solve solid phase ODE for $T_S(x)$

{$T_S(x)$ is the temperature distribution of the solid fuel}

If $T_s(x = x_{Eigen}) > T_{Eigen}$ **then**

$V_f \Leftarrow V_f - \omega$ {Reduce V_f}

else if $T_s(x = x_{Eigen}) < T_{Eigen}$ **then**

$V_f \Leftarrow V_f + \omega$ {Increase V_f}

else

{Eigen condition is satisfied}

endif

until {Eigen condition is satisfied}

$$\dot{m}''_F \Leftarrow \sqrt{\frac{\rho_s T_w^2 A_s \lambda_s R}{E_s\left[3.615\ \Delta h_v^0 + 4.605\ c_s(T_w - T_\infty)\right]}}\, e^{-E_s/2RT_w}$$

$$v \Leftarrow V_w = \frac{\dot{m}''_F}{\rho}$$

$$T \Leftarrow T_W = T_s\big|_{y=0}$$

STOP if convergence criteria satisfied for V_f

{Compare V_f with last 50 iterations and test if a convergence criterion is satisfied.}

Solve the gas phase PDE using SIMPLER algorithm of Patankar to find $T_g(x, y)$

$$\dot{q}''_{gsr}(x) \Leftarrow -\lambda_g \left.\frac{\partial T}{\partial y}\right|_{y=0}$$

endloop

Figure 18. Algorithm used to find the spread rate V_f

Table 1. Definition of terms used in the gas-phase canonical equation 1. B_g is the pre-exponential frequency factor of the Arrhenius equation for the gas-phase reaction $\frac{mm^3}{kg \cdot s}$.

Equation	ϕ	Γ_ϕ	$\dot{S}_\phi'''$
Continuity	1	0	0
x-momentum	u	μ	$-\frac{\partial}{\partial x} p + \rho g_x$
y-momentum	v	μ	$-\frac{\partial}{\partial y} p + \rho g_y$
Fuel mass	y_F	$\frac{\lambda_g}{c_{p,g}}$	$\dot{m}_F''' = -B_g \rho^2 y_O y_F e^{\frac{-E_g}{RT}}$
Oxygen mass	y_O	$\frac{\lambda_g}{c_{p,g}}$	$\dot{m}_O''' = -sB_g \rho^2 y_O y_F e^{\frac{-E_g}{RT}}$
Nitrogen mass	y_N	$\frac{\lambda_g}{c_{p,g}}$	0
Energy	T	$\frac{\lambda_g}{c_{p,g}}$	$-\frac{\dot{m}_F''' \Delta h_c^0 + \dot{q}_R'''}{c_{p,g}}$